International Journal of Thermophysics, Vol. 27, No. 2, March 2006 (© 2006)
DOI: 10.1007/s10765-005-0002-5

Solution of the Ornstein–Zernike Equation in the Critical Region

J. M. Brader[1]

Received January 18, 2005

A new numerical scheme for the solution of liquid state integral equations using the Baxter factorization of the Ornstein–Zernike equation is proposed. For short range potentials the method yields reliable results over the whole fluid region, including the vicinity of the critical point, and opens up new possibilities for numerical study of the critical behavior of integral equation approximations. To demonstrate the effectiveness of the method, numerical results are compared with the analytical solution of the mean spherical approximation for a hard-core plus Yukawa tail interaction potential. Accurate results for the critical exponents δ, γ, and η for this model are obtained.

KEY WORDS: critical exponents; integral equations; Ornstein–Zernike; thermodynamics.

1. INTRODUCTION

One of the fundamental challenges of liquid state theory is the calculation of bulk thermodynamics and structure given a particular model interaction potential. If the fluid structure lies close to that of hard spheres, then perturbation theory provides a good approximation for the pair correlations and thermodynamic quantities. The situation is less satisfactory if the interaction potential contains an attractive component, which causes the structure to deviate strongly from the reference system. In particular, if the system undergoes a liquid–gas transition, then perturbation theory yields an inadequate description of the critical region with mean-field values for the critical exponents. An alternative non-perturbative approach capable of trancending

[1] Universität Konstanz, Fachbereich Physik, D-78457 Konstanz, Germany. E-mail: jbrader@bell.physik.uni-konstanz.de

these difficulties is the method of integral equations, formed by approximate closures of the Ornstein–Zernike (OZ) equation. Integral equation approximations are essentially uncontrolled diagrammatic resummation schemes that can yield spectacular results in certain cases and are not necessarily mean-field in character. However, as most integral equations can only be solved numerically, assessing the critical behavior of a given integral equation is a non-trivial task.

The most familiar closures are the Percus–Yevick (PY), hypernetted-chain (HNC), and mean spherical approximation (MSA) [1–3]. Even for these relatively simple closures, there has been much confusion regarding the critical behavior. Important insight was gained from the analytical solution of the MSA for the special case of a pair potential with a hard-core plus attractive Yukawa tail (HCYF) [4, 5]. Extensive analysis of this solution confirmed that there exists a locus of points in the density–temperature plane along which the compressibility, as calculated from the long wavelength behavior of the structure factor, diverges, i.e., there exists a true spinodal line [6–8]. It was also confirmed that at the compressibility critical point the solution exhibits the expected mean spherical exponents but, due to the thermodynamic inconsistency of the approximate MSA pair correlation functions, the virial and energy routes exhibit mean field behavior. Comparisons between analytic and numerical results exposed the deficiencies of traditional numerical solution methods in the vicinity of the critical point and highlighted the need for extremely accurate numerical work when attempting to determine values for the critical exponents [9, 10]. No analogous analytical solution exists for the HNC equation, and we must rely on numerical results. In a detailed numerical study, Belloni [10] concluded, in contrast to previous findings, that the HNC approximation does not present a true spinodal curve but simply a region within which no convergent solution can be obtained. This region was previously identified with the spinodal due to the large values of the compressibility obtained on the boundary [11, 12]. Using a modified numerical algorithm, Belloni revealed that the compressibility, albeit large, remains finite everywhere and that the boundary line does not constitute a true spinodal curve. It follows that there exist no critical exponents for the HNC approximation. The critical behavior of the PY equation was also the subject of confusion following several numerical studies in which a divergence of the compressibility along the boundary line and mean-field values for the critical exponents were claimed [13–18]. The situation was greatly clarified by the existence of an analytic solution, in this case for the adhesive hard-sphere model of Baxter [19]. Baxter's solution was studied in detail by Fishman and Fisher [20], who confirmed the predicted mean-field exponents and the existence of a true spinodal line on the liquid side of

the critical point. However, the compressibility remains finite on the vapor side of the boundary line, in contradiction to the numerical findings. Subsequent numerical studies with improved resolution [21, 22] confirmed the analytic result.

The general picture which emerges is that unambiguous assessment from first principles of the critical behavior of a given integral equation closure requires extremely careful analysis, and that no general technique exists for such studies. The aim of the present work is to develop a general purpose numerical method which can be applied to an arbitrary integral equation closure to yield accurate results over the entire fluid region, including the vicinity of the critical point, without need for any supplementary analytical information. The paper will be structured as follows: In Section 2, we review and comment upon some existing schemes for numerical solution of integral equations with particular emphasis on the performance close to the critical point. In Section 3, we give details of the new algorithm. In Section 4, we compare our numerical results with the analytical results of the MSA for the HCYF and in Section 5, we discuss the significance of the results and suggest possible further developments.

2. NUMERICAL SOLUTION OF THE ORNSTEIN–ZERNIKE EQUATION

The OZ equation relates the direct correlation function $c(r)$ to the total correlation function $h(r)=g(r)-1$. In real space it can be written as

$$h(r)=c(r)+\frac{2\pi\rho}{r}\int_0^R \mathrm{d}x\; xc(x)\int_{|x-r|}^{x+r}\mathrm{d}y\; yh(y), \tag{1}$$

where $\rho\equiv N/V$ denotes the particle number density and $c(r)=0$ for $r>R$. We take the particle diameter σ as our unit of length. In Fourier space, the OZ equation is given by

$$\tilde{h}(q)=\frac{\tilde{c}(q)}{1-\rho\,\tilde{c}(q)}, \tag{2}$$

where $\tilde{c}(q)$ is the Fourier transform of $c(r)$. When supplemented by an independent relation between $h(r)$ and $c(r)$ (a closure relation), the OZ relation yields a closed integral equation for the pair correlation functions of the system. Although a formal closure is known in terms of an infinite series of integrals over $h(r)$ [23], this series is not useful for practical implementation. Integral equation theories attempt to approximate this

complicated functional relationship by a simpler local algebraic relation between $c(r)$ and $h(r)$.

2.1. Standard Algorithms

The simplest method of numerical solution is Picard iteration [1]. When using the real space form Eq. (1) initial guesses $c_0(r)$ and $h_0(r)$ are made and inserted into the R.H.S. This yields a new estimate $h_1(r)$ which is input to the closure relation to yield an improved estimate $c_1(r)$. This procedure usually only converges at low densities, and in order to obtain convergence at higher densities, it is necessary to mix old and new estimates to obtain a converged solution [1, 24, 25]. When using the Fourier space version Eq. (2), an analogous procedure can be followed by incorporating a numerical Fourier transform. In practice, Eq. (2) is generally preferred due to the fast-Fourier-transform (FFT) algorithm which can be used to avoid time consuming evaluation of real space convolutions [26]. A significant improvement upon direct iteration was made by Gillan [27], who developed a hybrid technique combining Picard iteration with the Newton–Raphson method. The resulting algorithm and subsequent refinements [28] provide not only vastly increased convergence rates but also prove more stable than straightforward iteration. An even more efficient algorithm using Newton–Raphson alone was proposed by Zerah [29]. All of these improved schemes make use of the Fourier space version Eq. (2).

Despite the success of these algorithms, there remains an intrinsic limitation of all methods-based directly on Eqs. (1) and (2). It is known that for short-range potentials the function $c(r)$ is of shorter range than $h(r)$ [1]. However, it is apparent from Eq. (1) that although full solution of the problem requires information only within the range $(0, R)$ [the range over which $c(r)$ is non-zero], an asymptotic form must be assumed for $h(r)$ over the range $(R, 2R)$. In practice, the condition $h(r)=0$ for $(R, 2R)$ is usually employed and yields accurate results at non-critical statepoints, provided that R is chosen sufficiently large. The problem occurs upon approaching the critical point. At the critical point, the correlation length, ξ, diverges, and $h(r)$ becomes long ranged, thus invalidating the assumption that $h(r)=0$ in the range $(R, 2R)$ for any finite choice of R. The situation becomes worse if Eq. (2) is used. Close to the critical point, $\tilde{h}(q)$ exhibits a high and narrow peak of width $\sim \xi^{-1}$. In order to correctly resolve this peak, the numerical Fourier transforms within the iterative cycle require a grid spacing $\Delta q \equiv 2\pi/R < \xi^{-1}$, which is violated as $\xi \to \infty$. Insufficient resolution of the low q behavior of $\tilde{h}(q)$ leads to incorrect values of $c(r)$ at low r values and subsequent inaccuracies in calculating the compressibility.

2.2. Ornstein–Zernike Technique

To correct these failings, Belloni [10] considered a modified version of Zerah's algorithm [29] in which analytic reference functions are subtracted and added before and after the numerical Fourier transform (the OZ technique). In the case of the MSA closure, both the small q behavior of $\tilde{h}(q)$ and large r behavior of $h(r)$ are known and can be used to self-consistently impose the correct asymptotics within each numerical cycle. In this way, the resolution of the numerical MSA solution can be greatly improved in regions of high compressibility. For approximations which do not possess known asymptotic behavior, some approximate form must be assumed. In Ref. 10, Belloni employed the same MSA-type reference functions to study the HNC and PY boundary lines. This assumption was found to improve the resolution sufficiently to confirm the absence of a true spinodal in both cases. We can speculate that this is a consequence of the finite compressibility on the HNC and (partially) PY boundary lines, and that supplementing the numerical algorithm with approximate analytic expressions for the asymptotics is sufficient in such cases. Given an integral equation exhibiting true power law behavior, but with unknown pair correlation asymptotics, it is not clear to what extent the modified algorithm would continue to improve the resolution close to the spinodal.

2.3. Baxter Equation

Throughout all of these developments, a potential solution to the problem was already at hand in the little known papers of Watts [13, 30, 31] who employed a very different numerical scheme based on the analytic work of Baxter [32]. Using a Wiener–Hopf type analysis, Baxter derived an alternative form of the OZ equation which involves $h(r)$ and $c(r)$ only over the range $(0, R)$. Baxter's alternative form is given by

$$\begin{aligned} H(r) = \; & C(r) + 2\pi\rho \int_0^r \mathrm{d}s \int_0^s \mathrm{d}t\, H(t)H(s-t) \\ & + 4\pi\rho \int_0^R \mathrm{d}s\, C(s) \left[\int_0^s \mathrm{d}t\, H(t) - \int_0^{|r-s|} \mathrm{d}t\, H(t) \right] \\ & + 4\pi^2\rho^2 \int_0^R \mathrm{d}s\, C(s) \int_0^r \mathrm{d}t\, W(s,t), \end{aligned} \tag{3}$$

where $H(r) = rh(r)$, $C(r) = rc(r)$, and $W(s,t)$ is given by

$$\begin{aligned} W(s,t) &= \int_0^s \mathrm{d}v\, H(v) \int_{|s-t-v|}^{s-|t-v|} \mathrm{d}u\, H(u), \quad s > t \\ W(s,t) &= -W(t,s). \end{aligned} \tag{4}$$

This expression is fully equivalent to Eq. (1) under the assumptions that $c(r)=0$ for $r>R$ and that the spatial integral of $h(r)$ is absolutely convergent (a condition satisfied for any disordered fluid).

It is known that the exact $c(r)$ becomes long ranged in the vicinity of the critical point, so the condition that $c(r)=0$ for $r>R$ cannot be exactly satisfied for any finite choice of R. However, for short-ranged potentials, a numerical treatment based on truncation of $c(r)$ is certainly far superior to the truncation of $h(r)$ required by Eqs. (1) and (2). A good example of this is provided by the HNC approximation, for which the asymptotic tail $c(r)\sim h^2(r)/2$ clearly decays much faster than $h(r)$. For approximations with asymptotic behavior $c(r)\sim -\beta\phi(r)$ [33], where $\beta=1/k_BT$ and $\phi(r)$ is the pair potential, Eq. (3) can provide results of arbitrary accuracy. Watts used a Newton–Raphson method to solve the simultaneous equations arising from discretization of Eq. (3) and found that convergence could be obtained with as few as five or six iterations. This method was used to study the Lennard-Jones fluid within the PY and HNC approximations [13, 30, 31]. A copy of Watts code was also used by Henderson and Murphy [14] to study the critical region of the same model system in the PY approximation.

We have made a careful numerical evaluation of Eq. (3) using the Newton–Raphson method (following Watts [13]) and, for comparison, a new Picard iteration scheme. Taking the analytic solution of the MSA for the HCYF as a benchmark, we obtain excellent agreement for the structure and thermodynamics using both methods. The accuracy of the numerical solution does not deteriorate within the critical region, and the absolute error remains essentially constant over the entire fluid region of the phase diagram, exhibiting only a very gradual increase with density due to the increasing structure of the correlation functions. A particularly impressive feature of the Picard solution method is the stability when compared to an iterative solution of the original OZ equation Eq. (1). At all state points, it is possible to begin with an ideal-gas initial solution, $H(r)=C(r)=-r$ for $r<\sigma$, and achieve full convergence within fewer than 100 iterations. For densities greater than $\pi\rho/6\approx 0.2$, it is necessary to mix old and new solutions at each iteration. Using the Newton–Raphson method, we find that convergence generally occurs in fewer than 10 iterations, which is consistent with the observations of Watts. In general, the Newton–Raphson algorithm is marginally more stable than Picard iteration.

Unfortunately this method has some drawbacks. The primary difficulty is the high-computational load introduced by the multiple integrals, all of which must be evaluated in real space to avoid the problems of resolution in Fourier space discussed in Section 2.1. The most computationally

demanding task is evaluation of the matrix $W(s,t)$, which requires a double integration for each (s,t) pair. An associated limitation is the numerical accuracy with which the multiple integrals can be evaluated. To obtain results within practical time scales, it is necessary to compromise high-accuracy simply in order to reduce the number of grid points. Sufficient accuracy is generally achieved for grid spacings $\Delta r < 0.01\sigma$, which places practical limits on the maximum value of the cutoff R, which can be considered. For pair potentials requiring $R \sim 10\sigma$ or greater, this would seem to make the method unsuitable for large scale investigations requiring repeated solution of the OZ equation, e.g., calculation of the coexistence curve. On balance, we recommended Picard iteration rather than Newton–Raphson for the implementation of this method, as the slight increases in convergence rate and stability do not warrent the increased programming effort.

2.4. Baxter Factorization

Shortly after deriving Eq. (3), Baxter developed a second alternative version of the OZ equation [34]. The resulting expressions are considerably simpler than Eq. (3) due to the introduction of an additional auxiliary function which allows Eq. (1) to be decomposed into a pair of simultaneous equations. The new expressions are completely self-contained over the range $(0, R)$ and are given by

$$\begin{aligned} rh(r) &= -q'(r) + 2\pi\rho \int_0^r \mathrm{d}t\, q(t)(r-t)h(|r-t|), \\ rc(r) &= -q'(r) + 2\pi\rho \int_r^R \mathrm{d}t\, q(t)q'(r-t), \end{aligned} \tag{5}$$

where $q'(r)$ is the spatial derivative of the factor function $q(r)$. A straightforward derivation of Eq. (5) can be found in Appendix B of Ref. 1. This form has proved extremely useful for analytic work, but also forms a potential basis for a numerical algorithm. Using the analytical solution of the HCYF in the MSA it has been shown that the factorized equations, Eq. (5), possess additional, unphysical solutions which are not solutions of the original OZ equation, Eq. (1). Imposing the additional constraint that the pair correlation functions remain bounded is sufficient to eliminate these unphysical solutions [35]. The assumptions underlying Eq. (5) are the same as for Eq. (3), namely that $c(R) = 0$ for $r > R$ and that the integral of $h(r)$ remains finite, and so all the advantages of Eq. (3) in the vicinity of the critical point are retained. In addition, the factorized form eliminates the multiple integrals, which are so detrimental to the performance

of methods based on Eq. (3). The possibility of numerical implementation of Eq. (5) was first suggested by Watts [36], who reported a private communication from Baxter. However, the first attempt to implement such a scheme was only made much later by Cummings and Monson [37]. In this study, both Picard and Newton–Raphson schemes were devised but, due to problems of both accuracy and stability, the results were inconclusive. A very brief preliminary report of an apparently successful implementation of Eq. (5) is given in Ref. 38. Unfortunately, the authors do not give details of the numerical algorithm and only confirm the power law decay of $h(r)$ at the critical point. No further assessment was made.

3. NEW SOLUTION METHOD

We now give details of the new iteration scheme based on the factorized equations, Eq. (5). We first specialize to the case of pair potentials with a hard core, as this allows the clearest illustration of the method. Application to potentials with a softer repulsion is then straightforward. The cycle begins by taking the low-density forms of the functions c_i, h_i, q_i, and q_i' as initial guesses. Improved estimates are generated according to

$$rh_i(r) = -q'_{(i-1)}(r) + J_{(i-1)}(r), \quad r \geqslant \sigma, \tag{6}$$

$$rc_i(r) = -q'_{(i-1)}(r) + I_{(i-1)}(r), \quad r < \sigma, \tag{7}$$

$$q_i'(r) = -rh_{(i-1)}(r) + J_{(i-1)}(r), \quad r < \sigma, \tag{8}$$

$$q_i'(r) = -rc_{(i-1)}(r) + I_{(i-1)}(r), \quad r \geqslant \sigma, \tag{9}$$

where I and J are given by

$$I_i(r) = 2\pi\rho \int_r^R \mathrm{d}t\, q_i(t) q_i'(r-t), \tag{10}$$

$$J_i(r) = 2\pi\rho \int_0^r \mathrm{d}t\, q_i(t)(r-t) h_i(|r-t|). \tag{11}$$

The use of different terms of the factorization Eq. (5) to account for different spatial ranges stabilizes the iterative cycle. Using the fact that $q(R) = 0$, we obtain $q(r)$ from $q'(r)$ at each iteration using

$$q_i(r) = -\int_r^R \mathrm{d}t\, q_i'(t). \tag{12}$$

The missing information, $h(r)$ for $r < \sigma$ and $c(r)$ for $r > \sigma$, is obtained from the appropriate closure relation. For example, the MSA is implemented by imposing

$$h_i(r) = -1, \quad r < \sigma, \tag{13}$$

$$c_i(r) = -\beta\phi(r), \quad r \geqslant \sigma, \tag{14}$$

whereas the formally exact closure of the OZ equation is implemented using

$$h_i(r) = -1, \quad r < \sigma, \tag{15}$$

$$c_i(r) = -\beta\phi(r) - \ln[1 + h_{(i-1)}(r)] + b(r) + h_{(i-1)}(r), \quad r \geqslant \sigma, \tag{16}$$

where $b(r)$ is the bridge function. For potentials with a softer repulsion, the core condition Eq. (15) should be replaced with the appropriate closure condition on $h(r)$. In the exact case, Eq. (15) should be replaced by

$$h_i(r) = \exp[-\beta\phi(r) + h_{(i-1)}(r) - c_{(i-1)}(r) + b(r)] - 1, \quad r < \sigma. \tag{17}$$

In such cases, the value of σ is not clearly defined but, in practice, it is sufficient to choose a value below which the repulsive part of the potential dominates. For example, the commonly studied Lennard-Jones potential is given by

$$\phi(r) = 4\epsilon\left[\left(\frac{\sigma_{LJ}}{r}\right)^{12} - \left(\frac{\sigma_{LJ}}{r}\right)^{6}\right], \tag{18}$$

where σ_{LJ} and ϵ are parameters controlling the length scale and potential strength, respectively. We find that choosing $\sigma = \sigma_{LJ}$ provides well converged solutions at all state points outside the no-solution boundary. In Fig. 1, we compare results for $g(r)$ obtained using the new algorithm with those of a modified Newton–Raphson–Picard algorithm, based on Eq. (2), for a state point close to the triple point, $T^* \equiv k_B T/\epsilon = 0.72$, $\rho = 0.85$. We give results for both the HNC equation, obtained by setting $b(r) = 0$ in Eqs. (16) and (17), and the MHNC equation [39], for which $b(r)$ is approximated by the PY hard-sphere expression. The density entering the bridge function is treated as an adjustable parameter to enforce thermodynamic consistency. In both cases, the agreement between the two numerical methods is perfect. On approaching the critical point, differences emerge as the traditional algorithm begins to display erroneous finite-size effects resulting from truncation of $h(r)$. An alternative approach to solving Eq. (5) is to employ a continuous crossover function to impose Eq. (17) within the core region and Eq. (6) outside. Convergence is not sensitive to the details of this choice, but for stability, the closure relation should be used to determine new esimates for $h(r)$ inside the strongly repulsive region and $c(r)$ outside this region.

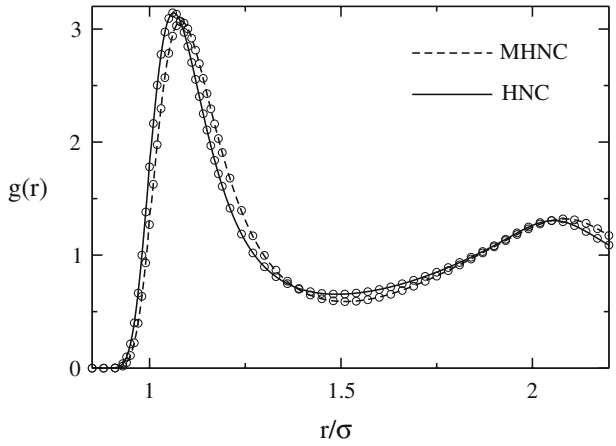

Fig. 1. Comparison of the results of the new algorithm (lines) with those of a modified Newton–Raphson–Picard method (circles) within the HNC and MHNC approximations for a Lennard-Jones fluid close to the triple point, $T^* = 0.72$, $\rho = 0.85$.

To monitor the level of convergence, we calculate the squared norm of $h(r)$ at each iteration

$$\int_0^\infty \mathrm{d}r[h_i(r) - h_{(i-1)}(r)]^2. \tag{19}$$

A value less than 10^{-11} usually ensures a well converged solution. When very high accuracy is required, i.e. when working close to the critical point, smaller values are necessary to guarantee a satisfactory solution. We have tested a range of different pair potentials and closures and find that convergence is generally achieved in fewer than 100 iterations, a result which is independent of proximity to the critical point. Using low-density initial solutions, it is necessary to mix old and new solutions but in all cases the stability and convergence is far superior to standard Picard iteration on the original form of the OZ equation. Iteration schemes based on Eq. (2) typically fail to converge for densities $0.1 < \pi\rho/6 < 0.14$ when ideal gas initial guesses are used without mixing, the precise details depending upon the interaction and the closure under consideration. In contrast, the new scheme can typically be used with no mixing up to a density of $\pi\rho/6 \approx 0.3$. We find that in many cases mixing as little as 45% of the solution from the previous iteration is sufficient to obtain convergence at all fluid densities, i.e. up to $\pi\rho/6 = 0.494$, from ideal gas initial solutions.

These observations suggest that Eq. (5) provides a more appropriate starting point for numerical work than Eq. (1). We also note that by starting with low-density initial guesses we did not encounter any difficulties with the unphysical solution branches known to exist for some closures (see e.g. Ref. 35). This suggests that such solutions may be unstable with respect to the current iterative solution scheme.

The reduced isothermal compressibility, $\chi_{\text{red}} = \rho k_B T \chi_T$, is usually calculated using the long wavelength limit of the Fourier transform of the direct correlation function, $\chi_{\text{red}}^{-1} = 1 - \rho \tilde{c}(0)$. It is a simple exercise to show that this standard definition is equivalent to

$$\chi_{\text{red}}^{-1} = \left(1 - 2\pi\rho \int_0^R \mathrm{d}t\, q(t)\right)^2. \tag{20}$$

We employ this alternative definition in our subsequent calculations as we find it to be less sensitive to numerical error than the standard relation.

4. COMPARISON WITH ANALYTIC RESULTS

In order to test the performance of our method in the vicinity of the critical point, we compare numerical results with the analytic solution of the MSA for the HCYF [4–8]. The HCYF is defined by the pair interaction

$$\begin{aligned} \beta\phi(r) &= \infty, \quad r < \sigma \\ &= -(K/r)\exp[-z(r-1)], \quad r \geqslant \sigma, \end{aligned} \tag{21}$$

where K is a parameter controlling the strength of the attraction (expressed in units of $k_B T$) and z sets the range of the potential. We consider the value $z = 2$ for which the liquid–gas coexistence curve is known to be strongly stable with respect to the freezing transition. To provide a demanding test of our algorithm, we focus on the exponents δ, γ, and η which describe the divergence of χ_{red} along the critical isotherm, the divergence of χ_{red} along the critical isochore and the decay of the total correlation function $h(r)$, respectively. The exponents are defined by

$$\begin{aligned} &\chi_{\text{red}} \sim |\Delta\rho|^{1-\delta}, && T = T_{\text{crit}}, \\ &\chi_{\text{red}} \sim |t|^{-\gamma}, && \rho = \rho_{\text{crit}}, \\ &h(r) \sim r^{-1-\eta}, && T = T_{\text{crit}}, \qquad \rho = \rho_{\text{crit}}, \end{aligned} \tag{22}$$

where $\Delta\rho = \rho/\rho_{\text{crit}} - 1$ and $t = T/T_{\text{crit}} - 1$. The MSA is known to yield mean spherical values for the exponents, $\delta = 5$, $\gamma = 2$, and $\eta = 0$ [8]. In order to obtain numerical estimates of the exponents, we consider the following *effective* exponents.

$$\delta_{\text{eff}} = -\frac{\mathrm{d}(\ln \chi_{\text{red}})}{\mathrm{d}(\ln \Delta\rho)} + 1, \qquad \gamma_{\text{eff}} = -\frac{\mathrm{d}(\ln \chi_{\text{red}})}{\mathrm{d}(\ln t)},$$
$$\eta_{\text{eff}} = -\frac{\mathrm{d}(\ln h(r))}{\mathrm{d}(\ln r)} - 1. \tag{23}$$

Upon approaching the critical point sufficiently closely, the effective exponents become equal to the true exponents. The third relation for η_{eff} refers to the asymptotic long-range behavior of $h(r)$. Analysis of the effective exponents also gives useful information regarding the extent of the asymptotic region about the critical point.

Figure 2 shows the numerically determined spinodal for $z = 2$ in the reduced density–temperature plane. Our numerical routine yields values of χ_{red} as high as 10^{20} on the boundary, from which it can be concluded with some confidence that the MSA possesses a true divergence on the spinodal boundary. The arrows in the figure indicate the paths taken in order to calculate the effective exponents δ_{eff} and γ_{eff}. In Fig. 3a, we show the inverse fourth root of χ_{red} as a function of ρ along the numerically determined critical isotherm. In order to identify the critical point, we calculate $\chi_{\text{red}}^{-1/4}$ as a function of ρ for increasing values of K. The point at which this curve first touches the axis upon increasing K identifies the critical density ρ_{crit}. Our best numerical estimate of the critical point is $\pi\rho_{\text{crit}}/6 = 0.1659785$, $K_{\text{crit}} = 1.1143650$, which is in excellent agreement with the exact values $\pi\rho_{\text{crit,ex}}/6 = 0.165978$, $K_{\text{crit,ex}} = 1.114384$, and demonstrates the

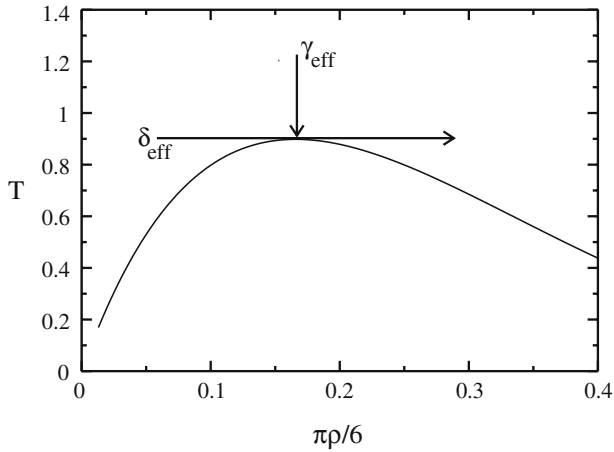

Fig. 2. The numerically determined spinodal line for the HCYF in the MSA for $z = 2$. The vertical axis is the reduced temperature $T = 1/K$. Arrows indicate the paths taken to identify the exponents δ and γ.

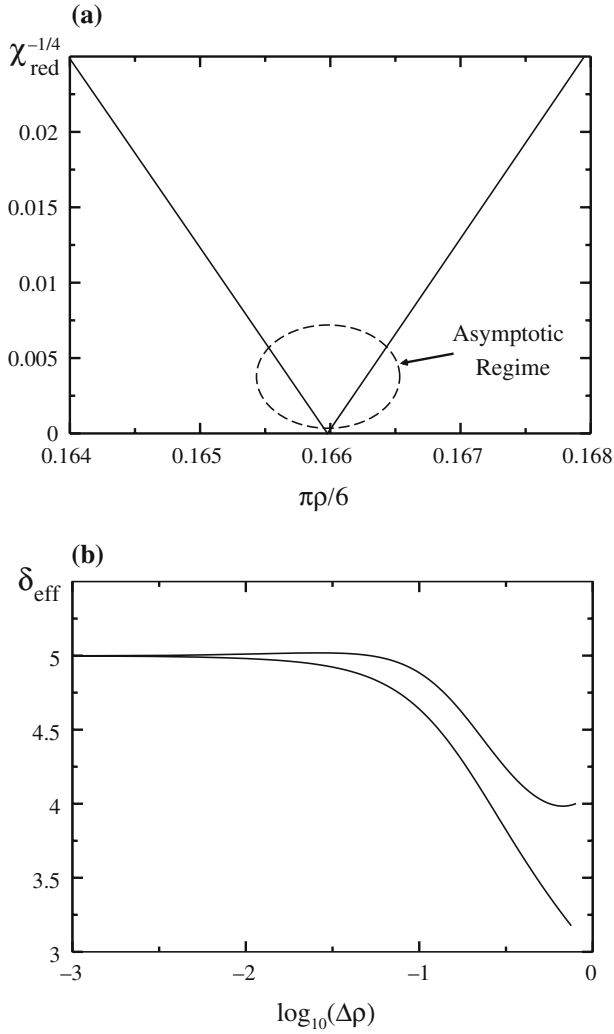

Fig. 3. Numerical determination of the exponent δ (a) Shows the fourth root of the inverse isothermal compressibility along the numerically determined critical isotherm. The linear behavior is consistent with the analytic result $\delta = 5$. The critical region in which δ assumes its exact value is indicated with an ellipse (b) Shows the effective exponent $\delta_{\text{eff}} = -\mathrm{d}(\ln \chi_{\text{red}})/\mathrm{d}(\ln \Delta\rho) + 1$ as a function of the logarithm of the reduced density $\Delta\rho = (\rho/\rho_{\text{crit}} - 1)$. As the critical point is approached, δ_{eff} saturates to the value $\delta = 5$.

resolution attainable using the new algorithm. The apparently linear behavior on either side of the critical point suggests a value $\delta = 5$. In Fig. 3b, we analyze this behavior more closely by plotting δ_{eff} as a function of reduced distance in density from the numerical critical point. As the critical point is approached, δ_{eff} saturates, unambiguously identifying the mean-spherical value $\delta = 5$ in accordance with the exact solution. The two branches in this figure correspond to sections of the isotherm above and below ρ_c. In calculating this result, we experimented with a number of different values for the cutoff R, gradually increasing the value until no appreciable changes occured in the solution. For non-critical statepoints, a value of $R \sim 6\sigma$ was found to be sufficient for the present value of z. Close to the critical point, this value had to be extended significantly. The solution at the critical point was found to stabilize for $R > 10\sigma$. In the present case, $c(r)$ is given analytically for $r > \sigma$ from which it follows that $c(R) < 10^{-9}$ for $r > 10\sigma$. It appears that $c(r)$ must assume values very close to zero in the vicinity of the cutoff in order for the method to yield highly accurate results near the critical point. For the present calculations, we use a grid spacing $\Delta r = 0.01\sigma$ and cutoff value $R = 10\sigma$.

Figure 4a shows χ_{red} as a function of reduced temperature distance from the critical point along the numerically determined critical isochore on a log scale. As the critical point is approached, the dependence becomes linear. In Fig. 4b, we examine this dependence more closely and show γ_{eff} as a function of $\log_{10}(t)$. For values of $t < 10^{-3}$, the effective exponent saturates to the mean-spherical value $\gamma = 2$ as expected. We find the identification of γ somewhat easier than of δ as the saturation limits of the effective exponent are less sensitive to errors in the location of the critical point. An approach along isochores for which ρ_{crit} is perturbed by a small amount yields saturating curves very similar to Fig. 4a, all of which give a value $\gamma = 2$. In contrast, the effective exponent δ_{eff} shown in Fig. 3b is sensitive to errors in ρ_{crit} and K_{crit}.

We next analyze the quality of the numerically determined $h(r)$ by comparison with the analytic expression of Kahl [40]. Figure 5a shows both the numerical total correlation function $h(r)$ and the exact function evaluated at the numerical critical point. The two curves are indistinguishable on the scale of the figure. The inset focusses on the region from $r = 2\sigma \to 6\sigma$ and clearly shows the onset of the asymptotic decay for $r \sim 5\sigma$. This figure should be contrasted with Fig. 5 in Ref. 9, which displays the discrepancies in $h(r)$ typical of traditional solution algorithms when applied in the critical region. In particular, the decay of the asymptotic tail is perfectly captured up to the cutoff value R using our new algorithm. In Fig. 5b, we show η_{eff} as a function of distance obtained from the critical $h(r)$. For $r \sim 6\sigma$, the effective exponent saturates to the mean-spherical value of zero.

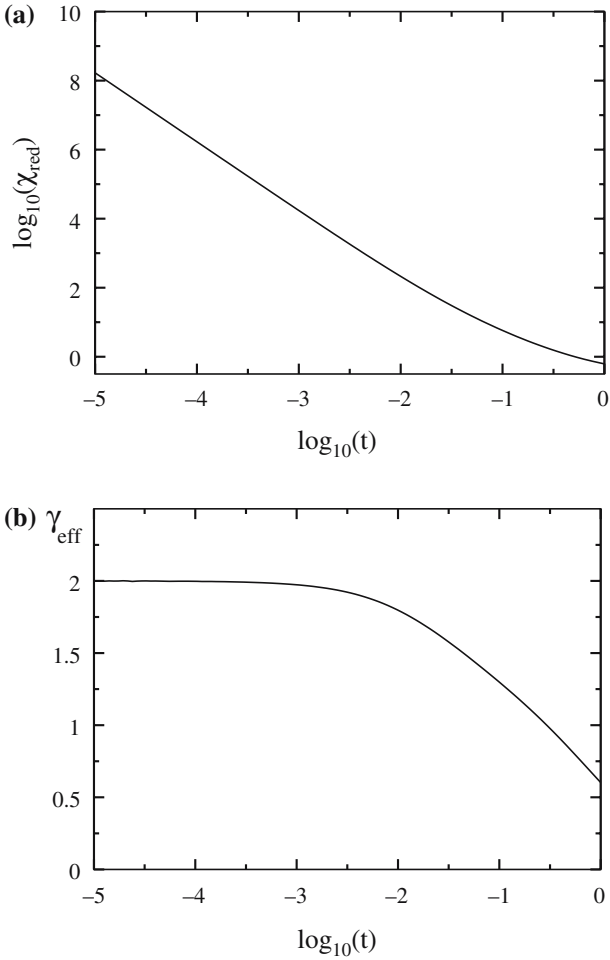

Fig. 4. Numerical determination of the exponent γ. (a) shows the logarithm of the reduced compressibility as a function of $\log_{10} t$, where $t = T/T_c - 1$. (b) shows the effective exponent $\gamma_{\text{eff}} = -\mathrm{d}(\ln \chi_{\text{red}})/\mathrm{d}(\ln t)$ as a function of $\log_{10} t$. As the critical point is approached, γ_{eff} saturates to the analytic value $\gamma = 2$.

5. DISCUSSION

We have presented a new numerical algorithm for solution of the OZ equation which, for short-range potentials, remains accurate in the vicinity of the critical point. By using the Baxter factorization, Eq. (5), as a basis for our method, we bypass the difficulties caused by the divergence of the correlation

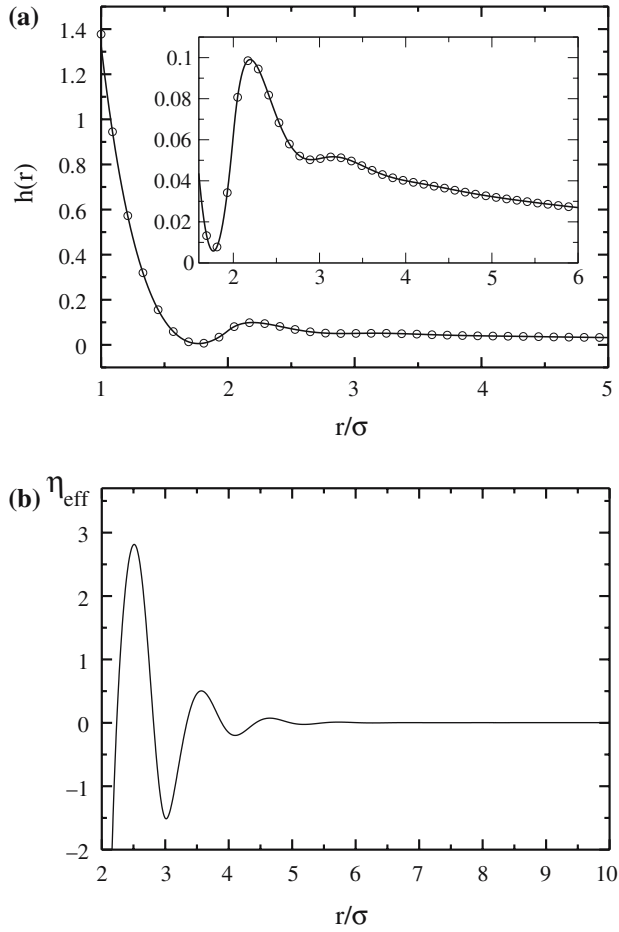

Fig. 5. Numerical determination of the exponent η. (a) compares the numerical $h(r)$ (line) with the analytic result (circles) at the numerically evaluated critical point $\pi\rho_c/6 = 0.1659785$, $K_c = 1.1143260$. The inset gives a more detailed view of the onset of the asyptotic decay in $h(r)$. (b) shows the effective exponent $\eta_{\text{eff}} = -\mathrm{d}(\ln h(r))/\mathrm{d}(\ln r) - 1$ as a function of r. The asymptotic behavior confirms the analytic result $\eta = 0$.

length upon approaching the critical point. The method is very stable and should facilitate future studies of the critical behavior of new integral equation approximations. The true values of the exponents are currently believed to be $\delta \approx 4.8$, $\gamma \approx 1.24$, and $\eta \approx 0.1$ [41]. The fact that the present algorithm can resolve correctly the MSA values $\delta = 5$, $\gamma = 2$, and $\eta = 0$ suggests that it will

indeed be useful for analyzing new integral equation approximations which aim to improve the description of the critical region.

We would like to emphasise that any criticism made of established numerical solution algorithms applies purely to the critical region. At state points removed from the critical point, for which the truncation of $h(r)$ is not restrictive, we find the hybrid [27, 28] and Newton–Raphson [29] techniques to be both fast and accurate, and we fully recommend them. The fact that our new algorithm does not employ the FFT naturally makes it slower than methods based on Eq. (2) [although it remains much faster than methods based on (3)]. It may therefore be useful to consider the development of a two-stage algorithm, which first solves the integral equation using a hybrid or Newton–Raphson method based on Eq. (2) and then refines this solution, if neccessary, by using the new algorithm. A simple approach would be to monitor the compressibility obtained from the first stage to determine whether refinement is necessary. In this way, one may take advantage of the existing optimizations while retaining accuracy close to the critical point.

Many more sophisticated closures have been proposed which attempt to improve upon the HNC, PY, and MSA [1, 3]. The most common source of improvement comes from the enforcement of thermodynamic consistency between two of the three thermodynamic routes (energy, virial, or compressibility) by including an additional variational parameter in the theory. Analysis of thermodynamically consistent theories in the critical region is more difficult than for the traditional closures due to the increased computational demands. Our new algorithm can be easily incorporated into such schemes and the accuracy it provides, particularly in regions of high compressibility, may well be advantageous when solving the consistency relations. It is often the case that thermodynamic consistency is imposed locally using exact relations between either the compressibility and the density derivative of the virial pressure or between the temperature derivative of the compressibility and the second density derivative of the internal energy [42]. All of these quantities can be evaluated from simple spatial integrals over functions containing density or temperature derivatives of $h(r)$ and $c(r)$. These correlation function derivatives are readily obtained by solving the coupled linear integral equations which result from direct differentiation of Eq. (5). This local procedure of evaluation is superior to the common finite difference approximation to the derivative obtained by solving the OZ equation at closely neighboring state points. Our preliminary results suggest that this method yields highly accurate results for the quantities $\partial P_{\text{virial}}/\partial\rho$, $\partial^2 u_{\text{ex}}/\partial\rho^2$, and $\partial\chi_{\text{red}}^{-1}/\partial T$, where P_{virial} is the virial pressure and u_{ex} is the excess internal energy per unit volume, required by many consistency schemes. The use of our new

algorithm in solving thermodynamically consistent approximations will be the subject of further investigation.

Although the verification of the MSA exponents using our algorithm is very satisfactory, the extent of the asymptotic region surrounding the critical point for a given integral equation is generally not known. Our results for the HCYF in the MSA suggest that our algorithm can yield accurate results for the effective exponents for values of $\Delta\rho$ and t as low as 10^{-4}. However, we are aware of an example for which the true asymptotic behavior only occurs for smaller values. The self-consistent Ornstein–Zernike approximation (SCOZA) of Høye and Stell [43–45], and Pini et al. [46] is a modification of the MSA, which incorporates a local thermodynamic consistency between the energy and compressibility routes. The full numerical solution required for an arbitrary pair potential is still an open problem, but for the special case of a HCYF one can take advantage of the analytical MSA solution to yield a quasi-analytic theory, which can be studied arbitrarily close to the critical point [46]. Note that in this case, solution of the OZ equation is performed analytically, and the theory is released from the numerical difficulties addressed in this paper. Figure 5 in Ref. 46 is the analogue of our Fig. 4 and shows the effective exponent γ_{eff} as a function of reduced temperature. Although the curve appears to begin saturation to a value close to the exact exponent when $t \sim 10^{-2}$, it is not until $t \sim 10^{-6}$ that the curve truly saturates and the genuine exponent, $\gamma = 2$, is revealed. For a theory requiring numerical solution of the OZ equation, such an extremely low value of t would appear prohibitive at the present time. The situation may be relieved to some extent by using shorter range potentials to investigate the critical behavior of a given closure. It is known that for the HCYF, reducing the potential range (increasing z) enlarges the size of the asymptotic regime [47], and thus determination of the exponents should not require such high-numerical resolution.

REFERENCES

1. J. P. Hansen and I. R. McDonald, *The Theory of Simple Liquids* (Academic, New York, 1986).
2. J. A. Barker and D. Henderson, *Rev. Mod. Phys.* **48**:587 (1976).
3. C. Caccamo, *Phys. Rep.* **274**:1 (1996).
4. E. Waisman, *Mol. Phys.* **25**:45 (1973).
5. J. S. Høye and L. Blum, *J. Stat. Phys.* **16**:399 (1978).
6. P. T. Cummings and E. R. Smith, *Chem. Phys.* **42**:241 (1979).
7. P. T. Cummings and E. R. Smith, *Mol. Phys.* **38**:997 (1979).
8. P. T. Cummings and G. Stell, *J. Chem. Phys.* **78**:1917 (1983).
9. P. T. Cummings and P. A. Monson, *J. Chem. Phys.* **82**:4303 (1985).

10. L. Belloni, *J. Chem. Phys.* **98**:8080 (1993).
11. P. D. Poll and N. W. Ashcroft, *Phys. Rev. A* **35**:866 (1987).
12. J. J. Brey and A. Santos, *Mol. Phys.* **57**:149 (1986).
13. R. O. Watts, *J. Chem. Phys.* **48**:50 (1968).
14. D. Henderson and R. D. Murphy, *Phys. Rev. A* **6**:1224 (1972).
15. M. I. Guerrero, G. Saville, and J. S. Rowlinson, *Mol. Phys.* **29**:1941 (1975).
16. J. J. Brey, A.Santos, and F. Romero, *J. Chem. Phys.* **77**:5058 (1982).
17. J. J. Brey, A. Santos, and L. F. Rull, *Phys. Rev. A* **26**:2993 (1982).
18. J. J. Brey and A. Santos, *J. Chem. Phys.* **82**:4312 (1985).
19. R. J. Baxter, *J. Chem. Phys.* **49**:2770 (1968).
20. S. Fishman and M. E. Fisher, *Physica (Utrecht)* **108A**:1 (1981).
21. F. Gallerani, G. Lo Vecchio, and L. Reatto, *Phys. Rev. A* **31**:511 (1985).
22. F. Gallerani, G. Lo Vecchio, and L. Reatto, *Phys. Rev. A* **32**:2526 (1985).
23. G. Stell, in *Equilibrium Theory of Classical Fluids* (Benjamin, New York, 1064).
24. A. A. Broyles, *J. Chem. Phys.* **33**:456 (1960).
25. K. C. Ng, *J. Chem. Phys.* **61**:2680 (1974).
26. W. H. Press, B. P. Flannery, S. A. Teukolsky, and W. T. Vetterling, *Numerical Recipes* (Cambridge University Press, Cambridge, 1986).
27. M. J. Gillan, *Mol. Phys.* **38**:1781 (1979).
28. S. Labik, A. Malijevsky, and P. Vonka, *Mol. Phys.* **56**:709 (1985).
29. G. Zerah, *J. Comp. Phys.* **61**:280 (1985).
30. R. O. Watts, *J. Chem. Phys.* **50**:1358 (1969).
31. R. O. Watts, *J. Chem. Phys.* **50**:984 (1969).
32. R. J. Baxter, *Phys. Rev.* **154**:170 (1967).
33. G. Stell, *Phys. Rev.* **184**:135 (1969).
34. R. J. Baxter, *Aust. J. Phys.* **21**:563 (1968).
35. G. Pastore, *Mol. Phys.* **731**:4 (1988).
36. R. O. Watts, in *Statistical Mechanics* Vol. **1** (Chemical Society Specialist Periodical Reports, London, 1973).
37. P. T. Cummings and P. A. Monson, *Int. J. Thermophys.* **11**:97 (1990).
38. P. Pińero, L. F. Rull, J. J. Morales, and J. M.Velarde, *J. Comp. Phys.* **88**:490 (1990).
39. Y. Rosenfeld and N. W. Ashcroft, *Phys. Lett.* **73A**:31 (1979).
40. G. Kahl, *Mol. Phys.* **67**:879 (1989).
41. A. M. Ferrenberg and D. P. Landau, *Phys. Rev. B* **44**:5081 (1991).
42. C. Caccamo, G. Pellicane, D. Costa, D. Pini, and G. Stell, *Phys. Rev. E* **60**:5533 (1999).
43. J. S. Høye and G. Stell, *J. Chem. Phys.* **67**:439 (1977).
44. J. S. Høye and G. Stell, *Mol. Phys.* **52**:1071 (1984).
45. J. S. Høye and G. Stell, *Int. J. Thermophys.* **6**:561 (1985).
46. D. Pini, G. Stell, and N. B. Wilding, *Mol. Phys.* **483**:95 (1998).
47. A. Borge and J. S. Høye, *J. Chem. Phys.* **108**:4516 (1998).